Microstructure, Atomic Bonds, and Dielectric Characteristics of Neodymium (Nd)-doped Barium Titanate

Iriani, Yofentina
Department of Physics, Faculty of Mathematics and Natural Sciences, Universitas Sebelas Maret

Suherman, Bachtiar
Department of Physics, Faculty of Mathematics and Natural Sciences, Universitas Sebelas Maret

Dianisa Khoirum Sandi
Department of Physics, Faculty of Mathematics and Natural Sciences, Universitas Sebelas Maret

Nurosyid, Fahru
Department of Physics, Faculty of Mathematics and Natural Sciences, Universitas Sebelas Maret

他

https://doi.org/10.5109/7236851

出版情報：Evergreen. 11 (3), pp.2063-2070, 2024-09. 九州大学グリーンテクノロジー研究教育センター
バージョン：

Microstructure, Atomic Bonds, and Dielectric Characteristics of Neodymium (Nd)-doped Barium Titanate

Yofentina Iriani[1,*], Bachtiar Suherman[1], Dianisa Khoirum Sandi[1], Fahru Nurosyid[1], Erfan Handoko[2]

[1]Department of Physics, Faculty of Mathematics and Natural Sciences, Universitas Sebelas Maret, Indonesia

[2]Department of Physics, Faculty of Mathematics and Natural Sciences, Universitas Negeri Jakarta, Indonesia

*Author to whom correspondence should be addressed:
E-mail: yofent_iriani@staff.uns.ac.id

(Received October 28, 2023: Revised May 23, 2024: Accepted June 21, 2024).

Abstract: Undoped and Neodymium (Nd)-doped Barium Titanate ($BaTiO_3$ or BT) with the general formula $Ba_{1-x}Nd_xTiO_3$ (where x = 0.00, 0.05, 0.10, and 0.20) were synthesized by the co-precipitation techniques to study their microstructure and dielectric characteristics. The X-ray Diffraction (XRD) examination revealed that the undoped BT was tetragonal while Nd-doped BT structures were cubic. The positions of (101) main peaks shifted slightly with the change in doping concentrations. The other phases of impurities were observed in all Nd-doped samples. The lattice parameter, crystallite size, and tetragonality did not alter linearly with increasing Nd concentration due to Nd valency and oxidation state changes. FTIR spectra validated the attendance of Ba, Ti, and O contents in all undoped and doped samples and impurities in the Nd-doped samples. The density values of all Nd-doped samples were all higher than the undoped BT. The dielectric constant of the samples also varied with increasing Nd concentration, which was associated with the changeable crystal structure condition and the presence of impurities. The undoped BT demonstrated the highest dielectric constant of 906 due to its absence of impurity. Subsequently, the dielectric constants of Nd-doped samples were 426 (x=0.05), 809 (x=0.10), 610 (x=0.15), and 787 (x=0.20).

Keywords: Barium titanate; Neodymium (Nd)-doped Barium; crystal structure; atomic bonds; density; dielectric constant

1. Introduction

Technological developments in sustainable and renewable energy have overgrown and prompted the exploration of high-performance energy storage systems[1-5]. Ferroelectric materials are one type of material that is often developed and applied. They have spontaneous polarization without the influence of an external electric field. In electronic devices, ferroelectrics are commonly applied to capacitors, Multi-Layer Ceramic Capacitors (MLCC), and Ferroelectric Random Access Memory (FRAM)[6-8]. Barium titanate ($BaTiO_3$ or BT) has become one of the most preferred ferroelectrics to study. It is an ABO_3 perovskite structure[9,11] that consists of octahedral oxygen as the center, an A-site containing Ba^{2+} ions with an ionic radius of 1.35Å, and a B-site containing Ti^{4+} ions with an ionic radius of 0.64Å[9,10]. BT has a high dielectric constant, so it is often used in many applications[13,14].

However, the properties of BT, especially the ferroelectric and piezoelectric properties, can be enhanced by doping[15-18]. Nowadays. Rare earth metals are attractive materials for use as dopants and are being studied. The metals include La^{3+}, Pb^{2+}, Na^{+}, Ga^{2+}, Nd^{3+}, and Cr^{4+}, which are commonly used to occupy the A-site[12]. In the B-site, Zr^{4+}, Fe^{3+}, Al^{3+}, In^{3+}, Cr^{3+}, Nb^{5+}, Ta^{5+}, Sb^{5+}, W^{6+} ions are used as doping materials. Among these, Neodymium is an interesting dopant. It has been observed that Nd^{3+} can replace Ba^{2+} and Ti^{4+} in BT[18]. Further, it is reported that Neodymium could affect the electrical properties and microstructure of BT[19,20]. Further, the dielectric characteristics of BT can be improved by Nd^{3+} doping[21].

Nd-doped BT has received significant attention from researchers such as Sasikumar et al.[22], Zhang et al.[23], and Ganguly et al.[24]. Sasikumar et al.[22] reported the synthesis of Nd-doped BT ($Ba_{1-x}Nd_xTiO_3$; x=0.00, 0.02, 0.04, 0.06, 0.08) via solid-state reaction. They found that the ferroelectric characteristics gradually declined after x=0.04 due to the transformation from a tetragonal to a cubic system. Zhang et al.[23] fabricated Nd-doped Barium via a hydrothermal method and discovered the improvement of the dielectric properties. Ganguly et al.[24]

have successfully synthesized $Ba_{1-x}Nd_{2x/3}TiO_3$ (x=0.00 – 0.10) ceramics with the solid-state reaction method. The results demonstrated a phase transition from tetragonal to cubic structure, a decrease in the Curie temperature, remnant polarization, and coercive field with an increase in Nd^{3+}.

Even though studies concerning the influences of Nd doping on BT properties have been conducted, many have not been reported regarding the fabrication process of Nd-doped BT, especially with the co-precipitation method and the impacts of Nd doping on BT characteristics.

The co-precipitation technique is a chemical method that combines two distinct solid and liquid materials[12,25,26]. The technique is simple and accurate for obtaining organic nanoparticles and avoiding unwanted deposits[7,27]. The co-precipitation method at room temperature reveals the benefits of low energy, shorter synthesis time, and safer and better synthesis results[28-30]. Besides, it does not require high pressure and airtight conditions[29]. The manufacture of powders with small particle sizes and uniform distribution usually could be achieved using this method.

Therefore, this work aims to investigate the impact of the mole concentration of Nd doping on the crystal structure, atomic bonds, and dielectric constant of Barium Titanate. The mole concentrations of doping used in this study were 5%, 10%, 15%, and 20%.

2. Method

The materials employed were Barium Hydroxide [$Ba(OH)_2$] (Sigma Aldrich 95%), Oxalic Acid Dihydrate [$C_2H_2O_4.2H_2O$] (Merck 99%), Titanium Tetrabutoxide (Sigma Aldrich 97%), Neodymium (III) Nitrate Hexahydrate [$Nd(NO)_3.6H_2O$], and Isopropanol (IPA). Synthesis of Nd-doped BT employed the co-precipitation method. The starting materials were weighed, and the mass of each material was computed based on the stoichiometry formula of $Ba_{1-x}Nd_xTiO_3$, where x is the mole concentration of Nd. The mole concentrations of Nd^{3+} dopants were varied at 0%, 5%, 10%, 15%, and 20%; accordingly, the samples were then coded as BT, BN5T, BN10T, BN15T, and BN20T for each mole concentration, respectively.

First, Oxalic Acid Dihydrate and Titanium Tetrabutoxide were disjointedly diluted in Isopropanol (IPA). The results were Solution 1 (Oxalic Acid Dihydrate + IPA) and Solution 2 (Titanium Tetrabutoxide + IPA). The two solutions were then mixed to obtain Solution 3. Afterward, Barium Hydroxide and Neodymium (III) Nitrate Hexahydrate were mixed in Solution 3. Then, distilled water was given to the solution, and the mixture was titrated. The titration method was by dropwise distilled water into Solution 3. The addition of distilled water drop by drop aims to achieve the dissolution of $Ba(OH)_2$ and $Nd(NO)_3.6H_2O$, and the system moved from a non-aqueous position to a semi-aqueous one. Next, the resulting titrated solution was left and precipitated for 24 hours at room condition. The precipitated solution was cleansed using ethanol and distilled water. Afterward, the hydrolysis process was carried out on the solution by heating it at 100ºC for 10 hours to obtain a powder. Finally, the powder was then heated at 900°C for 4 hours.

The powder samples were then characterized for their crystal structure, chemical bonds, and dielectric properties. The crystal structure characterization employed XRD D8 Advance Diffractometer Bruker USA with Cu-kα radiation, λ = 1.5406 Å, and the data analysis used the Rietveld refinement process using GSAS software. Further, the measure, theoretical, and relative densities of all samples were also computed. Fourier Transform Infrared (FTIR) Shimadzu IF Prestige 21 was performed to investigate the chemical bond, and the data analysis was conducted by observing the spectra peaks with a reference book. At the same time, the dielectric constant was measured via LCR Meter LCR-800 Series Gwinsteak. For dielectric property characterization, the powder was formed in bulk by means of a hydraulic press with 100 MPa pressure. It was coated then with silver paste to serve as electrodes.

3. Results and Discussion

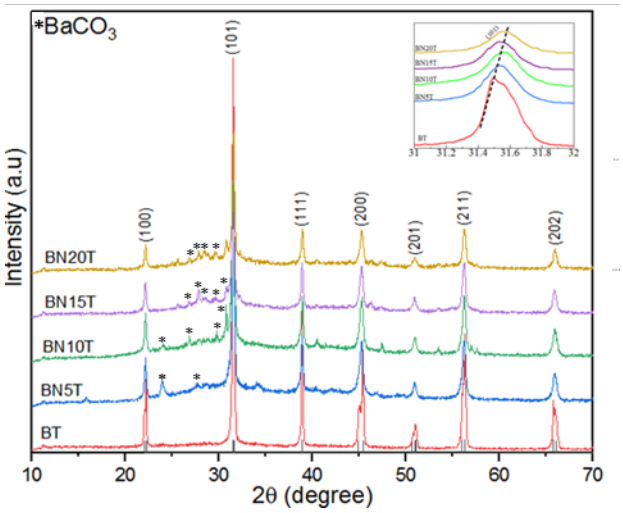

Fig. 1. Diffraction pattern of BT and Nd-doped BT with various Nd concentrations. Inset: the magnification peaks of (101) planes

Figure 1 presents the XRD results of BT and Nd-doped BT samples with variations in Nd concentrations. The emergent peaks were matched against the ICDD (International Center For Diffraction Data) database with PDF#831880, and the peaks were found to belong to the BT phase. As for x = 0.5 – 0.2, the patterns were agreed with a pure cubic phase of BT corresponding to ICDD file No. 00-31-0174. These findings were similar to those in the study conducted by Rejab et al.[31], where Nd-doped BT (Nd concentrations of 0.03 – 0.13) synthesized with the sol-gel method belonged to the cubic phase of BT[31].

Further, Figure 1 also shows other peaks with marks (*) identified as the $BaCO_3$ impurity phase. Zhang et al.[32] have also synthesized Nd-doped BT, where the concentration of Nd varied and ranged from 0.0005 to 0.05. It revealed that the impurity was only detected at the highest concentration of 0.05[32]. This condition was similar to that of this research, in which at the Nd concentration of 0.05, the impurities and their peaks got higher as higher Nd concentrations emerged. The appearance of this impurity might be due to the incomplete reaction of all starting materials during the sintering process[33]. The lack of Ti^{3+} or Ti^{4+} ions might also cause the emergence of $BaCO_3$ because the lack of Ti ions causes Ba^{2+} to react with CO_2 in the air[34]. Impurities have a terrible impact because they affect the material's performance, such as a decrease in the dielectric constant.

Further, the inset of Figure 1 is the magnification of (101) planes of all samples. It is apparent that giving Nd doping moves the diffraction peaks of (101) to the right. However, if all plane-related peaks were magnified, and the peaks' movement was inconsistent, some shifted to the right and others to the left. The move could indicate a change and inconsistency in the crystal structure as Nd doping, specifically in the lattice constant[35, 36].

The peak information from XRD was then examined with the Rietveld refinement process using the GSAS software to obtain information on the crystal structure (lattice constant, cell volume, crystallite size, and tetragonality). The results are shown in Fig. 3 and Table 1. Based on the figure, the black graph represents the graph from the XRD data (or observed data), while the red is from parameters taken in the ICDD database (or calculated data). The distinction between the two is the blue line. The green line is the background. The GSAS processing is done through background refinement to approximate the calculated curves close to the observed ones. So that, a small Chi2 (χ^2) value (< 2) is obtained until convergence is formed. It is seen from the refinement results that the diffraction peaks follow the ICDD database. Table 1 also exhibits that the χ^2 values obtained were less than 2.

Table 1. χ^2, lattice constant (a, b, c), cell volume (V), crystallite size (D), and tetragonality (c/a) of BT and Nd-doped BT samples

	BT	BN5T	BN10T	BN15T	BN20T
χ^2	1.864	1.874	1.920	1.867	1.998
Crystal System	Tetragonal	Cubic	Cubic	Cubic	Cubic
a=b(Å)	3.9802	4.0044	3.9988	3.9865	3.9934
c(Å)	4.0119	-	-	-	-
V (Å^3)	63.56	64.21	63.93	63.35	63.68
D (nm)	39	30	27	32	31
(c/a)	1.0079	1	1	1	1

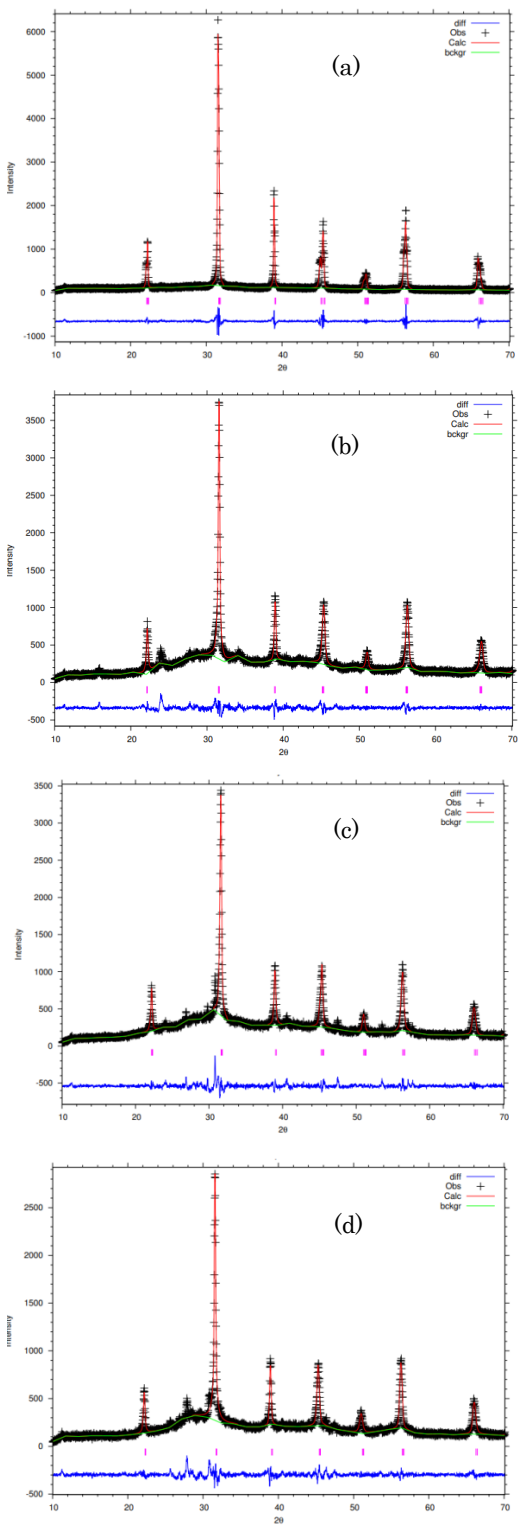

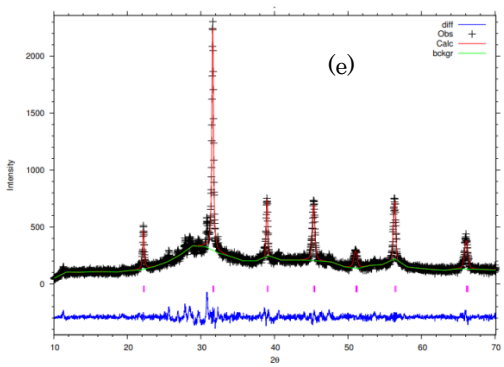

Fig. 2. Rietveld refinement of (a) BT; (b) BN5T; (c) BN10T; (d) BN15T; (e) BN20T

According to Table 1, it is found from the refinement process that all samples have a tetragonal structure. Table 1 also shows the lattice constants, cell volumes, tetragonality, and crystallite sizes of all samples. The lattice constant of the material increases with 5% Nd concentration from BT; it then tends to decrease at 10% and 15% Nd doping, and it slightly increases at 20% decreases. These yields were similar to those reported by Rejab et al. [31], with the Nd concentration from 0 – 0.13. Similarly, Zhang et al.[32] said similar yields with Nd concentration from 0.0005 to 0.05. The reasons were not mentioned clearly. Still, another report explained that it appeared that Nd substitutes at both Ba and Ti sites due to the ionic radius of Nd, which is almost exactly midway between those of Ba and Ti (Ba^{2+}=1.36 Å, Nd^{3+} = 0.98 Å and Ti^{4+}=0.605 Å)[22,23]. The cell volume also enlarges from BT to BN10T and turns to shrink slightly at BN15T. Meanwhile, for the crystallite size, it shrinks from BT to BN10T and turns to enlarge at 15%Nd and 20%Nd. For tetragonality, it reduces from BT to BN15T and slightly increases at BN20T. Thus, it is inferred that not all crystal structure parameters are linearly modified with increasing Nd concentration. The undependable valance of Nd can be associated with these occurrences[37]. Besides, it also can be caused by the changes in the oxidation state of Nd ions[38].

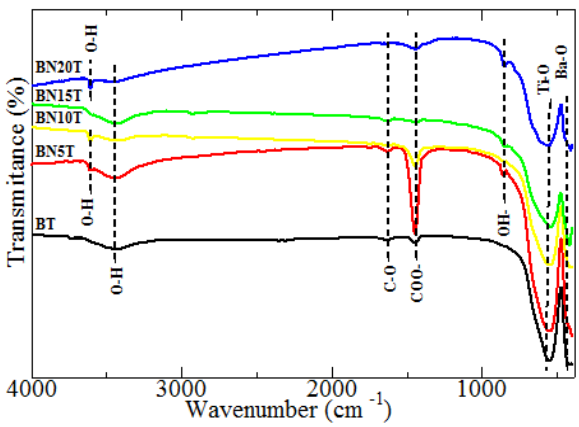

Fig. 3. FTIR spectra of BT and Nd-doped BT with variation in Nd concentrations

Figure 3 displays FTIR spectra of all samples at wavenumbers of 350 – 4000 cm^{-1}. Based on the figure, the prominent stretching vibrations around wave numbers 542 cm^{-1} and 432 cm^{-1} denote the presence of Ti-O and Ba-O bonds. Thus, it confirms the successful formation of the $BaTiO_3$ perovskite structure in this study[29]. Then, several vibration peaks are detected at wavenumbers around 3606 cm^{-1}, 3430 cm^{-1}, and 854 cm^{-1}, which refer to O-H groups. The peak vibration at wavenumber around 1444 cm^{-1} is identified as COO- bond. The wavenumber about 1627-1634 cm^{-1} is detected as the stretching vibration of the C–O bond, indicating the impurity of $BaCO_3$[39]. However, increasing the concentration of Nd doping could reduce the C–O vibration peak. This aligns with the XRD results and research conducted by Sun et al. (2017)[7]. $BaCO_3$ appeared because the sample was sintered at 900°C. $BaCO_3$ is removed perfectly at temperatures above 1600 K (~1327°C)[40]. Furthermore, the absence of a vibration peak of Nd in the FTIR spectra reveals that doping has been successfully incorporated into the BT structure because doping does not change the host structure.

The theoretical density (ρ_t), the measured density (ρ_m), and the relative density (ρ_{rel}) of all samples were also estimated according to work in[36] through the formulas as Equation (1-3). In which m, v, M, V, and N_A are the mass of the sintered bulks, the volume of the sintered bulks, the molecular mass of BT, the unit cell volume, and Avogadro's number, respectively. From the equation, the value of ρ_t only relies on the unit cell volume of each sample, meaning that a large unit cell volume leads to small ρ_t, and vice versa. Meanwhile, for the ρ_e, the value depends on the condition of the bulk after being sintered.

$$\rho_m = m/v \quad (1)$$

$$\rho_t = M/V\,N_A \quad (2)$$

$$\rho_{rel} = \rho_m/\rho_t\, x\, 100\% \quad (3)$$

The calculation results are presented in Table 3. Overall, the addition of the Nd dopant increases the values of the three densities. A high and uniform density is a fundamental requirement for a material with a high dielectric constant[42].

Figure 4 presents the dielectric constant of all samples. The dielectric constant value was from a frequency range of 1 kHz-100 kHz. Typically, all ferroelectric materials show the same phenomena where the dielectric constant increases at lower frequencies and decreases at higher frequencies. Polarization gradually declines and becomes stable with an improvement in frequency, where the space charge and dipole cannot follow the electric field at a very high frequency; consequently, there is no movement in the dipole, so the dielectric reduces[41,43].

Table 4 demonstrates the dielectric constants of all samples. Subsequently, the highest dielectric constant is achieved by pure BT samples, followed by BN10T,

BN20T, BN15T, and BN5T. The dielectric property depends on several aspects, including crystallite size, grain size, density or porosity, material impurities, etc.[28,37]. The larger crystallite and grain sizes will result in a higher dielectric constant because they give more space for dipoles to move. Further, the higher density will yield a higher dielectric constant because it provides more charges than a more porous surface.

Table 3. Measured density, theoretical density, and relative density of BT and Nd-doped BT

Parameters	BT	BN5T	BN10T	BN15T	BN20T
ρ_m(g/cm^3)	5.63	9.15	8.91	8.87	8.56
ρ_t (g/cm^3)	6.11	9.75	9.77	9.89	9.84
ρ_{rel} (%)	92.2	93.86	91.2	89.64	86.99

Table 4. The dielectric constant of $BaTiO_3$ and Nd-doped BT

Parameter	BT	BN5T	BN10T	BN15T	BN20T
Dielectric Constant	907	426	809	610	787

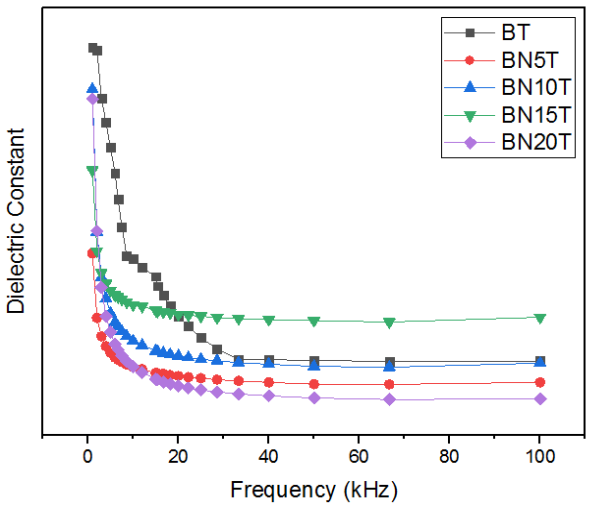

Fig. 4. Dielectric Constants of $BaTiO_3$ and Nd-doped BT

If seen, even though it does not possess the largest crystallite size nor the densest surface, the undoped BT exhibits the highest dielectric constant than other doped samples. Hence, it might be considered that the undoped BT reveals no impurity, based on XRD and FTIR data, compared to the doped samples. Also, it is stated in[43] that the dielectric constant in the doped barium titanate material declines with the presence of other phases or impurities. Zhang et al. also report similar results where the dielectric constant of BT dropped as the incorporation of Nd by x=0.005 – 0.05, revealing that pure BT possessed the highest dielectric constant[32]. As we know, various aspects impact the dielectric properties of BT. As for this case, the decrease in the dielectric constant was considered due to the phase transformation change from cubic to tetragonal phase and the decline in the tetragonality (c/a ratio) decrease caused by Nd doping[23, 24, 32]. Figures 5 and 6 present the relations between the dielectric constants, the crystallite size, and tetragonality as the function of the Nd concentrations.

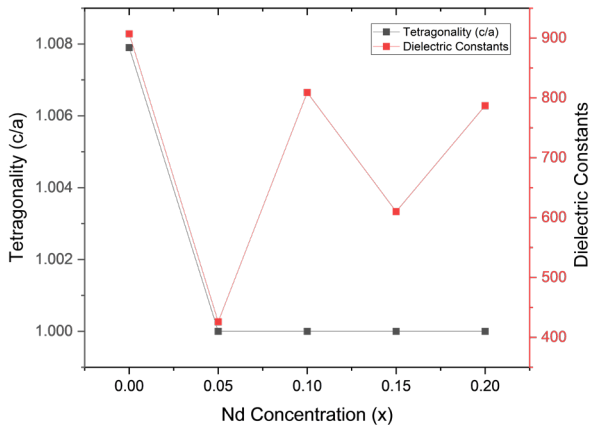

Fig. 5. The relations between the dielectric constants and tetragonality as the function of the Nd concentrations

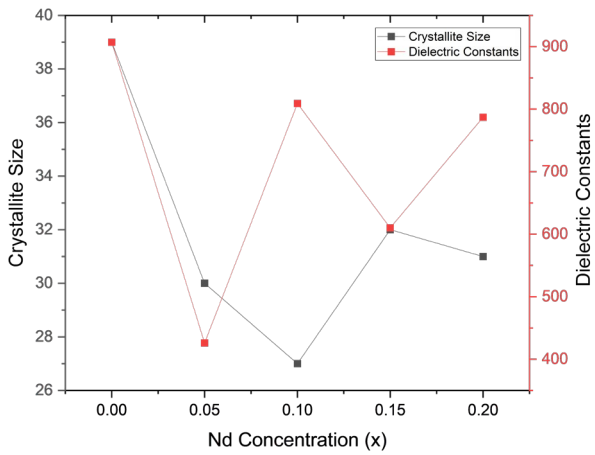

Fig. 6. The relations between the dielectric constants and crystallite size as the function of the Nd concentrations

4. Conclusion

Nd-doped BT has been successfully synthesized with the co-precipitation method and a temperature of 900°C. XRD patterns validated the tetragonal phase for the undoped BT, changing to the cubic phase for Nd-doped BT accompanied by the appearance of impurities. FTIR spectra supported the XRD results, which exhibited the atomic bonds of Ba, Ti, and O for all samples and the addition of impurities for Nd-doped samples. The density values of Nd-doped samples were higher than the BT. Nevertheless, the undoped BT gave the best results for the dielectric property due to the absence of impurities and the highest tetragonality.

Acknowledgments

Thanks to RKAT PTNBH Universitas Sebelas Maret for backup this research through Hibah Unggulan Terapan with number 254/UN27.22/PT.01.03/2022.

References

1) A. R. Nurohmah, C. S. Yudha, M. Rahmawati, S. S. Nisa, A. Jumari, H. Widiyandari, and A. Purwanto," Structural and Electrochemical Analysis of Iron Doping in $LiNi_{0.6-x}Mn_{0.2}Co_{0.2}Fe_xO_2$ battery," *EVERGREEN Joint Journal of Novel Carbon Resource Sciences & Green Asia Strategy*, **8**(1), 82-88 (2021). https://doi.org/10.5109/4372263
2) S. P. Dwivedi, M. Maurya, and S. S. Chauhan, Mechanical, "Physical and Thermal Behaviour of SiC and MgO Reinforced Aluminium Based Composite Material," *EVERGREEN Joint Journal of Novel Carbon Resource Sciences & Green Asia Strategy,* **8**(2), 318-327, (2021). https://doi.org/10.5109/4480709
3) Y. Phanny and M. Todo, "Effect of Sintering Time on Microstructure and Mechanical Properties of Hydroxyapatite Porous Materials for Bone Tissue Engineering Application," *EVERGREEN Joint Journal of Novel Carbon Resource Sciences & Green Asia Strategy,* **1**(2), 1-4, (2014). https://doi.org/10.5109/1495025
4) S. Hirata and M. Ohtaki, "Simultaneous Enhancement in the Electrical Conductivity and Reduction in the Lattice Thermal Conductivity Leading to Enhanced Thermoelectric ZT Realized by Incorporation of Metallic Nanoparticles into Oxide Matrix," *EVERGREEN,* **07** (01) 01-06 (2020). https://doi.org/10.5109/2740934
5) M. M. Rahman, S. Saha, M. Z. H. Majumder, T. T. Suki, M. H. Rahman, F. Akter, M. A. S. Haque, M. K. Hossain, "Energy Conservation of Smart Grid System Using Voltage Reduction Technique and Its Challenges," *EVERGREEN,* **09** (04) 924-938 (2022). https://doi.org/10.5109/6622879
6) D. K. Sandi, A. Supriyanto, A. Jamaluddin, and Y. Iriani, "The effects of sintering temperature on dielectric constant of Barium Titanate ($BaTiO_3$)," *IOP Conference Series: Materials Science and Engineering*, **107**, 012069 (2016). doi.org/10.1088/1757-899X/107/1/012069
7) A. U. L. S. Setyadi, F. Nurosyid, and Y. Iriani, "Influence of holding time annealing process on the microstructure and optical properties of barium titanate ($BaTiO_3$) thin film using the sol-gel method," *AIP Conference Proceedings*, **2202**, 020024 (2019).doi.org/10.1063/1.5141647
8) R. Mahbub, T. Fakhrul, and M. F. Islam, "Enhanced dielectric properties of Tantalum Oxide doped Barium Titanate based ceramic materials. Procedia Engineering." **56**, 760–5 (2013). doi.org/10.1016/j.proeng.2013.03.191
9) T. Badapanda, V Senthil, S. Panigrahi, and S. Anwar," Diffuse phase transition behavior of dysprosium doped barium titanate ceramic," *Journal of Electroceramics*, 31, 55-60 (2013). doi.org/10.1007%2Fs10832-013-9808-x
10) R. P. Rini, F. Nurosyid, Y. Iriani, and D. Fasquelle, "The addition of bismuth (Bi) to the barium titanate ($BaTiO_3$) prepared by chemical solution deposition," *Journal of Physics: Conference Series*, **1825**, 012065 (2021). doi.org/10.1088/1742-6596/1825/1/012065
11) M. Singh, B. C. Yadav, A. Ranjan, M. Kaur, and S. K. Gupta,"Synthesis and characterization of perovskite barium titanate thin film and its application as LPG sensor," *Sensors and Actuators, B: Chemical*, **241**, 1170–8 (2017). doi.org/10.1016/j.snb.2016.10.018
12) Q. Sun, Q Gu, K. Zhu, R Jin, and J. Liu *et al*, "Crystalline Structure, Defect Chemistry and Room Temperature Colossal Permittivity of Nd-doped Barium Titanate," *Scientific Report*s, **7**, 1-8 (2017). doi.org/10.1038/srep42274
13) B. Bajac, J. Vukmirović, D. Tripković, E. Djurdjić, and J. Stanojev *et al*, "Structural characterization and dielectric properties of BaTiO3 thin films obtained by spin coating," *Processing and Application of Ceramics*, **8**, 4 (2014). doi.org/10.2298/PAC1404219B
14) P. Beena, and H. S. Jayanna, "Dielectric studies and AC conductivity of piezoelectric barium titanate ceramic polymer composites," *Polymers and Polymer Composites*, **27**, 9 (2019). doi.org/10.1177/0967391119856140
15) Z. Chchiyai, F. El Bachraoui, Y. Tamraoui, L. Bih, and A. Faik *et al*, "Design and characterization of novel manganite perovskites $Ba_{1-x}Bi_xTi_{1-x}Mn_xO_3$ ($0 \leq x \leq 0.2$)," *Ceramics International*, **46**, 26911-22 (2020). doi.org/10.1016/j.ceramint.2020.07.169
16) D. J. Kim, M. H. Lee, and T. K. Song, "Comparison of multi-valent manganese oxides (Mn^{4+}, Mn^{3+}, and Mn^{2+}) doping in $BiFeO_3$-$BaTiO_3$ piezoelectric ceramics." *Journal of the European Ceramic Society*, **39**, 4697-704 (2019). doi.org/10.1016/j.jeurceramsoc.2019.07.013
17) R. T. Setyadhani, A. Jamaluddin A, and Y. Iriani, "Effects of iron dopants on barium strotium titanate ($Ba_{0.8}Sr_{0.2}TiO_3$) thin films," *Advanced Materials Research,* 896, 229–32 (2014). doi.org/10.4028/www.scientific.net/AMR.896.229
18) Q. Liu, J. Liu, D. Lu, W. Zheng, and C. Hu, "Structural evolution and dielectric properties of Nd and Mn co-doped $BaTiO_3$ ceramics," *Journal of Alloys and Compounds,* 760, 31–41 (2018). doi.org/10.1016/j.jallcom.2018.05.089
19) M. Ganguly, S. K. Rout, P. K. Barhai, C. W Ahn, and I. W. KiM, "Structural, electrical, and optical

properties of $(Ba_{1-x}Nd_{2x/3})TiO_3$ ceramics," *Phase Transitions*, **87**, 157-74 (2014). doi.org/10.1080/01411594.2013.798411

20) Z. Raddaoui, R. Lahouli, S. E. L. Kossi, J. Dhahri, and K. Khirouni *et al*., "Effect of oxygen vacancies on dielectric properties of $Ba_{(1-x)}Nd_{(2x/3)}TiO_3$ compounds," *Journal of Alloys and Compounds*, **771**, 67-68 (2019). doi.org/10.1016/j.jallcom.2018.08.242
21) A. Marikani, V. Selvamurugan, G. Mangamma, S. Ravi, and R. Krishnasharma, "Ferroelectric, dielectric, and optical properties of Nd-substituted $Bi_4Ti_3O_{12}$ nanoparticles synthesized by sol-gel method," *Progress in Natural Science: Materials International*, **26**, 528-32 (2016). doi.org/10.1016/j.pnsc.2016.11.001
22) S. Sasikumar, T. K. Thirumalaisamy, S. Saravanakumar, S. A. Bahadur, D. Sivaganesh, and I. B. S. Banu, "Effect of neodymium doping in $BaTiO_3$ ceramics on structural and ferroelectric properties," *Journal of Materials Science: Materials in Electronics*, **31**, 1535–1546 (2020). https://doi.org/10.1007/s10854-019-02670-6
23) W. X. Zhang, L. X. Cao, G. Su, and W. Liu, " Influence of microstructure on dielectric properties of Nd-doped barium titanate synthesized by hydrothermal method," Journal of Material Science: Material Electron, **24**, 1801–1806 (2013). DOI 10.1007/s10854-012-1015-z
24) M. Ganguly, S. K. Rout, P. K. Barhai, C. W. Ahn, and I.W. Kim," Structural, electrical, and optical properties of $(Ba_{1-x}Nd_{2x/3})TiO_3$ ceramics," *Phase Transitions,* 157-174 (2013). https://doi.org/10.1080/01411594.2013.798411
25) Y. Subarwanti, R. D. Safitri, A. Supriyanto, Y. Iriani, and A. Jamaludin, "Variation of Strontium (Sr) in the Ferroelectric Material Barium Strontium Titanate $(Ba_{1-x}Sr_xTiO_3)$ by Co precipitation Method," *IOP Conference Series: Materials Science and Engineering*, **176**, 012044 (2017). doi.org/10.1088/1757-899X/176/1/012044
26) U. Ulfa, K. Kusumandari, and Y. Iriani, "The effect of temperature and holding time sintering process on microstructure and dielectric properties of barium titanate by co-precipitation method, "*AIP Conference Proceedings*, **2202** (2019). doi.org/10.1063/1.5141649
27) J. Wang, Y. Cheng, R. Peng, Q. Cui, and Y. Luo, "Co-precipitation method to prepare molecularly imprinted fluorescent polymer nanoparticles for paracetamol sensing," *Colloids and Surfaces A: Physicochemical and Engineering Aspects*, **587**, 124342 (2020). doi.org/10.1016/j.colsurfa.2019.124342
28) Z. Yang, P. Gredin, and M. Mortier, "Extremely straightforward room temperature co-precipitation method to synthesize cubic KYF4:Yb/Er up-conversion nanoparticles in deionized water-ethanol solution," *Optical Materials*, **98**, 109458 (2019). doi.org/10.1016/j.optmat.2019.109458
29) X. Zhang, J. Yue, Y. Zhao, Z. Yan, and G. Zhu, "Synthesis of tetragonal $BaTiO_3$ nanoparticle via a novel tartaric acid co-precipitation process," *Ceramics International*, **47**, 7263-7 (2021). doi.org/10.1016/j.ceramint.2020.11.006
30) M. D. Noviastuti, Y. Iriani, and K. Kusumandari, "Electrical Properties of Barium Titanate Doped Lanthanum $(Ba_{1-x}La_xTiO_3)$ Fabricated Using Co-precipitation Method," *IOP Conference Series: Materials Science and Engineering*, **578**, 1-7 (2019). doi.org/10.1088/1757-899X/578/1/012033
31) N. A. Rejab, S. Sreekantan, K. Abd Razak, and Z. A. Ahmad, "Structural characteristics and dielectric properties of neodymium-doped barium titanate," *Journal of Materials Science: Materials in Electronics*, **22**, 167-73 (2011). doi.org/10.1007/s10854-010-0108-9
32) W. Zhang, L. Cao, W. Wang, G. Su, and W. Liu, " Effects of neodymium doping on dielectric and optical properties of $Ba_{(1-x)}Nd_xTi_{1.005}O_3$ ceramics," *Ceramics – Silikáty*, **57** (2), 146-150 (2013).
33) M. A, Siddiqui, F. Hussain, M. S. Hanif, and A.A. Mohamad, "Effect of calcination and sintering temperatures on physical properties of barium titanate ceramic," *International Journal of Electroactive Materials*, **6**, 42-7 (2018).
34) N. N. Hasbullah, S. K Chen, K. B Tan, Z. A. Talib, and J. Y. C. Liew, "Photoluminescence activity of $BaTiO_3$ nanocubes via facile hydrothermal synthesis," *Journal of Materials Science: Materials in Electronics*," 30, 5149-75 (2019). doi.org/10.1007/s10854-019-00813-3
35) M. S. Alkathy, and K. C. James Raju, "Enhancement of dielectric properties and energy storage density of bismuth and lithium co-substituted strontium titanate ceramics," *Ceramics International*, **44**, 10367 (2018). doi.org/10.1016/j.ceramint.2018.03.049
36) W. Cai, C. Fu, J. Gao, and Deng X, "Effect of Mn doping on the dielectric properties of $BaZr_{0.2}Ti_{0.8}O_3$ ceramics," *Journal of Materials Science: Materials in Electronics*, **21**, 317-25 (2010). doi.org/10.1007/s10854-009-9913-4
37) T. Iqbal, M. Mustofa, M.S. Ishtiaque, M.J. Rahman, and S. Coudhury, "Effect of Ce-Mn codoping on the structural, morphological and electrical properties of the $BaTiO_3$ based ceramic," *Biointerface Research in Applied Chemistry*, **11**(4), 12215-12226 (2021). doi.org/10.33263/BRIAC114.1221512226
38) A. Rani, J. Kolte, and P. Gopalan, "Phase formation, microstructure, electrical and magnetic properties of Mn substituted barium titanate," *Ceramics International*, **41**, 14057-63 (2015). doi.org/10.1016/j.ceramint.2015.07.023
39) T. T. M. Phan, N. C. Chu, V. B. Luu, H. Nguyen Xuan, and D. T. Pham, "Enhancement of polarization

property of silane-modified $BaTiO_3$ nanoparticles and its effect in increasing dielectric property of epoxy/$BaTiO_3$ nanocomposites," *Journal of Science: Advanced Materials and Devices*, **1**, 90-7 (2016). doi.org/10.1016/j.jsamd.2016.04.005

40) M. D. A. Gomes, L. G. Magalhães, A. R. Paschoal, Z. S. Macedo, and Á. S. Lima, "An eco-friendly method of $BaTiO_3$ nanoparticle synthesis using coconut water," *Journal of Nanomaterials*, **2018**, (2018). doi.org/10.1155/2018/5167182
41) M. Arshad, H. Du, M. S. Javed, A. Maqsood, and I. Ashraf, "Fabrication, structure, and frequency-dependent electrical and dielectric properties of Sr-doped $BaTiO_3$ ceramics," *Ceramics International*. **46**, 2238-46 (2020). doi.org/10.1016/j.ceramint.2019.09.208
42) M. Kumari, N. Baraik, and P. M. Sarun, "Effect of Nd doping on the structural, optical and dielectric properties of $BaTi_{0.95}Sn_{0.05}O_3$ ceramics," *Journal of Alloys and Compounds*, **883**, 160635 (2021). doi.org/10.1016/j.jallcom.2021.160635
43) H. A. Gatea, and I. S Naji, "The effect of Ba/Sr ratio on the Curie temperature for ferroelectric barium strontium titanate ceramics." *Journal of Ovonic Research*, **14**, 467-74 (2018). doi.org/10.1142/S2010135X20500216